This is the accepted manuscript made available via CHORUS. The article has been published as:

Collisional decoherence and rotational quasirevivals in asymmetric-top molecules

Ian F. Tenney, Maxim Artamonov, Tamar Seideman, and Philip H. Bucksbaum

Phys. Rev. A **93**, 013421 — Published 25 January 2016

DOI: 10.1103/PhysRevA.93.013421

Collisional decoherence and rotational quasi-revivals in asymmetric-top molecules

Ian F. Tenney*

Department of Physics, Stanford University, Stanford, California 94305, USA and Stanford PULSE Institute, SLAC National Accelerator Laboratory, Menlo Park, California 94025, USA

Maxim Artamonov† and Tamar Seideman‡

Department of Chemistry, Northwestern University, Evanston, Illinois 60208, USA

Philip H. Bucksbaum§

Department of Physics, Stanford University, Stanford, California 94305, USA

Department of Applied Physics, Stanford University, Stanford, California 94305, USA and Stanford PULSE Institute, SLAC National Accelerator Laboratory, Menlo Park, California 94025, USA

Abstract

We demonstrate the observation of quasi-periodic revivals out to 27 ps in an impulsively-aligned asymmetric-top molecule, sulfur dioxide (SO_2), at high sample temperature and density (295 K, 0.5 bar). We find that the asymmetric top exhibits a strong correlation between population alignment and population lifetime ($r = 0.97$), in accordance with the trend observed in linear molecules. We use a linear birefringence measurement fit to a full quantum simulation of the asymmetric rotor, and are able to separately measure both the population (T_1) and coherence (T_2) lifetimes of the rotational wavepacket. Additionally, we observe a high rate of elastic decoherence ($T_2^* = 9.6$ ps), and attribute this to long-range interactions mediated by the permanent dipole of the SO_2 molecule. We propose the use of birefringence measurements to study intermolecular interactions in a coherent ensemble, as a step toward using field-free alignment to investigate reaction dynamics and dissipative processes.

* iftenney@stanford.edu

† m-artamonov@northwestern.edu

‡ t-seideman@northwestern.edu

§ phb@slac.stanford.edu

I. INTRODUCTION

A. Motivation

The methods and theory of molecular alignment provide a powerful tool for studying the rotational dynamics of excited molecules. In the gas phase, molecules normally exist in an isotropic state, yet on the level of an individual molecule most chemical and physical properties are strongly dependent on orientation. Field-free alignment with an ultrafast laser pulse allows for time-resolved measurements in the molecular frame, which provide critical insights for many areas of current research, including high harmonic generation (HHG) [1–6], x-ray scattering, and ultrafast chemical transformations [7].

Impulsive alignment has been well-studied both theoretically and experimentally in linear molecules such as nitrogen, carbon dioxide, and iodine [8–11]. These molecules exhibit regularly-spaced rotational energy levels $E \approx B \cdot J(J+1)$ that yield well-defined periodic "revival" features as quantum echoes of the post-pulse transient alignment [8–11]. The vast majority of molecules of interest, however, are not linear, but are asymmetric tops with three non-degenerate moments of inertia. In this case, the rotational Hamiltonian:

$$\hat{\boldsymbol{H}}_{rot}\psi = \frac{\hat{\boldsymbol{J}}^2}{2I} = \frac{1}{\hbar^2}\left(A\hat{\boldsymbol{J}}_a^2 + B\hat{\boldsymbol{J}}_b^2 + C\hat{\boldsymbol{J}}_c^2\right)\psi = E\psi. \tag{1}$$

where $A, B, C = 1/2I_{\{aa,bb,cc\}}$ are the rotational constants, is non-separable and generates complex, aperiodic rotational behavior [12–14]. In order to apply molecular alignment to many polyatomic systems of practical interest, it is necessary to understand, characterize, and measure the rotational dynamics of the asymmetric top.

Sulfur dioxide presents as an interesting target molecule for alignment due to its almost-prolate nature (asymmetry parameter $\kappa = \frac{(2B-A-C)}{(A-C)} = -0.942$, where $\kappa = -1$ is prolate-symmetric, $\kappa = +1$ is oblate-symmetric [14]). In this regime, the asymmetric rotor exhibits quasi-periodic revival features with sufficient coherence to obtain a clear signal, yet with enough asymmetry to show aperiodic dephasing effects and multiple-axis dynamics [14, 15]. Moreover, SO_2 carries a strong molecular dipole capable of long-range interactions [16], and a number of electronic properties, including an excited-state conical intersection that can be best studied in an aligned ensemble [1].

B. Previous Work

Previous work in impulsive alignment has focused on linear molecules such as N_2 and CO_2. Very high levels of transient, periodic (revival), and permanent (population) alignment have been achieved using optimal control theory [14, 17] and multiple-pulse trains [10, 18, 19], including measurements at high rotational temperature in the presence of centrifugal distortion [11]. Linear molecules have been aligned at high sample densities, and the decoherence properties of linear-molecule rotational wavepackets have been studied in detail [20–22].

Studies of asymmetric-top molecules, however, have been more narrow in scope. Most recent work has focused only on transient alignment, with the goal of achieving field-free three-dimensional alignment [19, 23, 24], for which SO_2 is a well-studied target. This approach holds promise for many applications, but does not permit the study of intermolecular interactions or other processes over multiple picosecond timescales.

Revivals in asymmetric tops have been studied under the framework of rotational coherence spectroscopy (RCS)[12], yet this work has been largely conducted in low-density, low-temperature molecular beams [13, 25, 26]. In this regime, collisional decoherence is minimized, and the small number of populated rotational states makes it easier to achieve coherences and to measure them with ionization-based techniques. Quasi-periodic revivals have been achieved in SO_2 [1] and molecules with a similar degree of asymmetry, including ethylene [6] ($\kappa = -0.914$ [14]) and iodobenzene [27, 28] ($\kappa = -0.965$ [14]) at moderate temperatures (50-200 K), yet the Coulomb explosion and HHG-based measurement techniques do not admit the study of high-density samples.

To the best of our knowledge, no studies to-date have investigated decoherence processes in asymmetric tops, nor studied them under conditions of high temperature and high density where decoherence plays significant role in the dynamics of a rotational ensemble. Understanding these processes is critical to controlling long-lived (> 10 ps) rotational wavepackets in dense samples, and provides a means to study intermolecular interactions on picosecond timescales [21, 22]. These interactions can include the transfer of angular momentum and rotational phase, both across a coherent ensemble as well as between different molecular species as mediated by collisions and long-range interactions [29, 30].

II. BACKGROUND

A. Impulsive Alignment

Impulsive alignment, or impulsive rotational Raman excitation, has become the technique of choice for studying rotational dynamics [31], due to the ability to achieve field-free alignment in a wide variety of molecules. A strong linearly- or circularly-polarized laser pulse with a duration much shorter than relevant rotational timescales ($t_{pulse} \approx 20 - 200\text{fs} \ll \tau_{rev}/J$) excites rotational transitions to create a coherent rotational wavepacket. If the pulse is longer than a vibration period and centered on an optical frequency (often near-IR) far from any vibrational or electronic transitions in the target molecule, then the excitation will consist solely of rotational Raman transitions stimulated by the pulse envelope [32].

This wavepacket evolves in time to yield a transient alignment peak shortly after the excitation pulse, followed by periodic or quasi-periodic "revivals" of this initial alignment as the coherent beat phase of the off-diagonal elements of the rotational density matrix ρ completes a full rotation. In the case of a linear molecule, these revivals are localized at a time $\tau_{rev} \approx 1/2B$ derived from the energy levels $E \approx B \cdot J(J+1)$ and the Raman selection rules $\Delta J = 0, \pm 2$, $\Delta M = 0$. The excitation also creates some degree of permanent alignment, whereby conservation of the magnetic quantum number M as J is increased creates a non-oscillating anisotropic component that appears as an elevated baseline in $\langle \cos^2(\theta) \rangle$ and other measures of ensemble alignment.

The wavepacket additionally evolves by interaction among molecules, both within the excited ensemble and with the surrounding environment. Elastic collisions scramble the phase of the off-diagonal elements, while inelastic collisions and radiative processes shed excess angular momentum and relax toward a thermal ensemble. These effects manifest as a time-decay of both the periodic and the permanent alignment features [22, 33].

B. The Asymmetric Top: Unique Challenges

In the case of an asymmetric-top molecule, the wavepacket is affected by additional confounding factors that distort from an "ideal" alignment behavior. First, unlike with linear and symmetric-top molecules, the rotational energy levels of an asymmetric top are irregularly spaced, and their beats do not superimpose as a harmonic series. Therefore,

the coherent excitation can create only quasi-periodic revivals as the different frequencies spread out and "dephase" over time [14, 15, 34]. Second, the reduced symmetry allows for relaxed selection rules for the quadrupole excitation ($\Delta J = 0, \pm 1, \pm 2$, $\Delta K = 0, \pm 2$, $\Delta M = 0$ [35, 36]), causing the coherences to be distributed over a larger number of rotational transitions. This generates a set of four distinct superimposed rotational series (Table I) involving all three molecular axes. Measuring this provides a richer signal that provides a source of three-dimensional molecular frame information [1], albeit at the expense of weaker features in any single channel.

Third, in relatively heavy molecules such as SO_2, significant populations in high-J states that occur at room temperature can make centrifugal distortion effects play an important role in the wavepacket dynamics. This has a similar effect as in linear molecules, reducing the harmonic properties of the rotational spectrum, and thus causing the revivals to weaken and spread out in time [11, 31]. Finally, many asymmetric-top molecules carry a permanent molecular dipole which can participate in long-range intermolecular interactions [16, 29, 30], which increases interaction cross-sections and accelerates the decoherence process. Taken together with collisional decoherence and population relaxation, these effects make observing a revival signal in an asymmetric-top more difficult than in a symmetric top or linear rotor, yet they also enable the measurement of multiple-axis contributions and the combined study of individual decoherence phenomena.

TABLE I. Rotational revival types, participating axes, and revival periods for sulfur dioxide, following the notation of Felker [12]. Times given are approximate due to lack of true periodicity, and axis contributions are derived from orthogonal modes in the symmetric-top limit, applied to the full asymmetric moment-of-inertia tensor.

Revival Type	**Primary Axes**	τ_{rev}, $\mathbf{SO_2}$
J-type	B,C	26 ps
K-type, Hybrid	A,B,C	4.9 ps, 9.8 ps
C-type	C	28 ps
A-type	A	4.1 ps

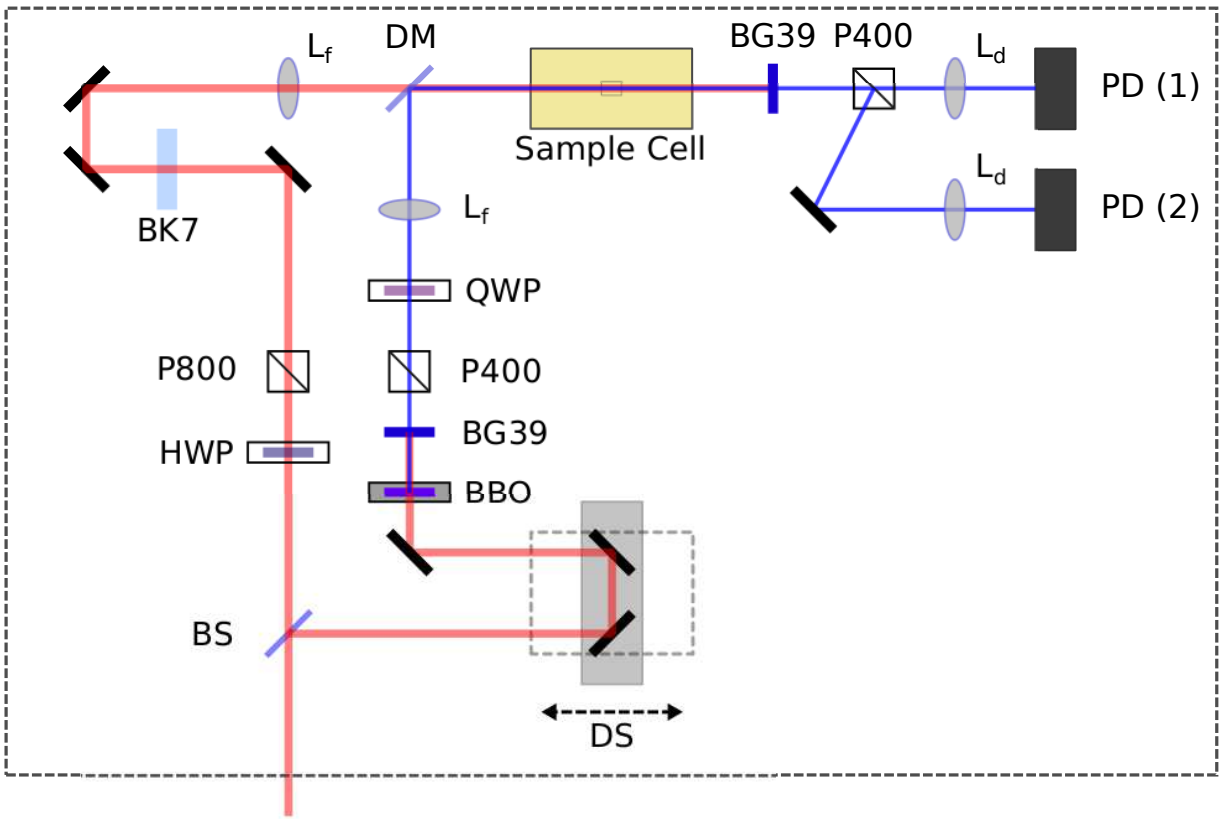

FIG. 1. (Color online) Experimental setup for impulsive alignment and birefringence polarization-gate measurement. The beam splitter (BS) splits the incoming light, bottom, into the pump (75% power) and probe beams (25% power). The pump beam is polarized vertically (S) to align to the lab z-axis, and passes through the HWP (half-wave plate) and P800 (Glan-Taylor polarizer) for variable attenuation. BK7: 10 mm BK7 glass slab to temporally stretch the pump pulse [a]. DS: delay stage. BBO: β-Barium Borate second-harmonic crystal. BG39: colored-glass filter, blocks 800 nm. P400: Glan-Laser polarizer. QWP: quarter-wave plate. L: focusing lenses, L_f = 200 mm, or L_d = 100 mm. DM: dichroic mirror (T800/R400). PD: Silicon photodiode detector, ϕ =10 mm. The second P400 acts as a polarizing beamsplitter to provide differential measurement. The beam diameter throughout is ∼6 mm.

[a] This reduces peak intensity, to minimize ionization in the sample.

III. METHODS

A. Impulsive Excitation

Figure 1 describes the optical setup for this experiment. Our sample is a sealed glass cell containing 0.5 bar of sulfur dioxide and a small amount of air as a reference, and maintained at the laboratory temperature of 295 K. We induce a rotational wavepacket using a 50-100 fs, 800 nm linearly-polarized pulse from a Ti:Sapphire laser system focused to an intensity of 20-55 TW/cm^2. In this regime, we are far from the electronic transitions in SO_2 ($\Delta E_{elec} > \approx 266$ nm), but significantly shorter than the J-type revival period of 26 ps. Therefore, we have that $\Delta E_{rot} \ll \hbar\omega \ll \Delta E_{elec}$, and so the effect of the pulse can be modeled as shown in [37] as the effect of the field envelope on the molecular dynamic polarizability tensor [32]:

$$\begin{aligned} \boldsymbol{V}(t) &= -\frac{1}{2}\vec{p}(t)\cdot\vec{\epsilon}(t) = -\frac{1}{2}\vec{\epsilon}(t)\cdot\overleftrightarrow{\alpha}\cdot\vec{\epsilon}(t) \\ &\approx -\frac{1}{4}\varepsilon^2(t)\left[\alpha_A\cos^2\theta_A + \alpha_B\cos^2\theta_B + \alpha_C\cos^2\theta_C\right] \end{aligned} \tag{2}$$

where $\vec{p}$ is the induced dipole vector, $\overleftrightarrow{\alpha}$ is the dynamic polarizability tensor, $\varepsilon(t)$ is the pulse field envelope, and $\vec{\epsilon}(t) = \Re\left\{\varepsilon(t)\cdot\hat{z}\cdot e^{i\omega t}\right\}$ is the electric field of the laser pulse. We can simplify this by subtracting the potential of the isotropic components, since this does not affect rotation, yielding:

$$\boldsymbol{V}_{eff}(t) = -\frac{1}{4}\varepsilon^2(t)\cdot\left[\Delta\alpha_A\cos^2\theta_A + \Delta\alpha_B\cos^2\theta_B\right] \tag{3}$$

in which we see that the field couples to the anisotropic components of the most-polarizable axes. For sulfur dioxide, these are the prolate O-O axis (A) and the C_2 symmetry axis (B), as shown in Figure 2, and in the classical picture the pulse can be thought of as exerting an instantaneous torque on these axes and exciting a complicated set of (unstable) rotations. In the full quantum picture, we model these as off-diagonal elements in the density matrix $\rho(t)$. We model the field interaction with the usual propagator [10, 14], yielding to first order:

$$\rho(t) = U(t,t_0)\rho(t_0)U(t,t_0)^\dagger \tag{4}$$

$$U(t,t_0) \approx \exp\left(\frac{-i}{\hbar}\int_{t_0}^{t}\left[\boldsymbol{H}_{rot} + \boldsymbol{V}_{eff}(t)\right]\ dt'\right) \tag{5}$$

where the diagonal matrix $\rho(t_0)$ is a thermal ensemble, and the off-diagonal elements introduced by the action of V can be grouped into the four rotational series described in Table I.

B. Birefringence Measurement

We measure the alignment with a birefringence polarization-gate measurement similar to Raman-Induced Polarization Spectroscopy (RIPS). We use a collinear pump-probe scheme as shown in Figure 3. The probe is a low-intensity (< 1 TW/cm^2) circularly-polarized 400 nm pulse set at a variable delay to the 800 nm pump using a mechanical stage. This pulse does not cause appreciable alignment itself, but experiences a measurable birefringence from the anisotropic ensemble by coupling to the same $\cos^2\theta$ matrix elements as the initial excitation. For a prolate molecule, alignment with the pump polarization $\hat{z}$ will create a

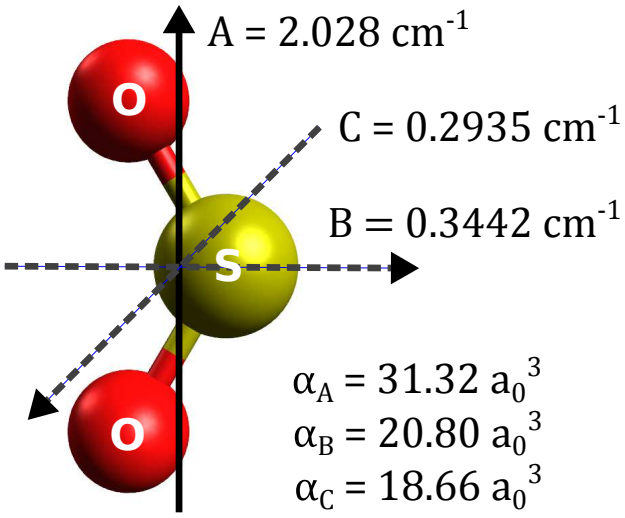

FIG. 2. (Color online) Rotational moments (A,B,C) and dynamic polarizabilities (α_A,α_B,α_C) for sulfur dioxide, as shown in the molecular frame. [38, 39]. Note that the C_{2v} symmetry of SO_2 guarantees that the molecular polarizability tensor $\overleftrightarrow{\alpha}$ is diagonal in the same basis as the rotational moment-of-inertia tensor.

slow axis in the laboratory frame (and conversely a fast axis perpendicular to it), which induces a phase shift that is linear in the alignment:

$$Signal = \boldsymbol{\delta} = \kappa \cdot \left[\Delta\alpha_A \left(\langle \cos^2 \theta_A \rangle - \frac{1}{3} \right) + \Delta\alpha_B \left(\langle \cos^2 \theta_B \rangle - \frac{1}{3} \right) \right] \tag{6}$$

where κ is a proportionality constant that depends on the gas density, refractive index, and effective optical path length [9]. As experienced by a circularly-polarized probe pulse, $\vec{E}_C(\hat{x}, t) = \Re \left\{ E_0 \frac{1}{\sqrt{2}} (\hat{y} + i\hat{z})\, e^{i(kx - \omega t)} \right\}$, this shift will distort the polarization to an ellipse. Measuring at $\pm 45^\circ$ gives a signal that, for small $\boldsymbol{\delta}$, is linear in the alignment metric of $\langle \cos^2 \theta \rangle$:

$$\begin{aligned} S_\pm &= \langle (\vec{E}_C \cdot \vec{p}_\pm)^2 \rangle = \frac{|E_0^2|}{4} \left(1 - \cos\left(\frac{\pi}{4} \pm \boldsymbol{\delta} \right) \right) \\ &= \frac{|E_0^2|}{4} \left(1 \pm \sin(\boldsymbol{\delta}) \right) \approx \frac{|E_0^2|}{4} \left(1 \pm \boldsymbol{\delta} \right) \quad \text{for} \quad \delta \ll 1 \end{aligned} \tag{7}$$

These signals are combined in a differential measurement scheme $\frac{(S_+ - S_-)}{(S_+ + S_-)} = \boldsymbol{\delta}$, which provides strong rejection of common-mode noise. This allows us to achieve a high dynamic range, allowing for investigation of weaker features such as K-type revivals, and, critically, providing the robust baseline subtraction necessary to accurately measure population alignment and relaxation. Furthermore, it decouples the alignment signal from other

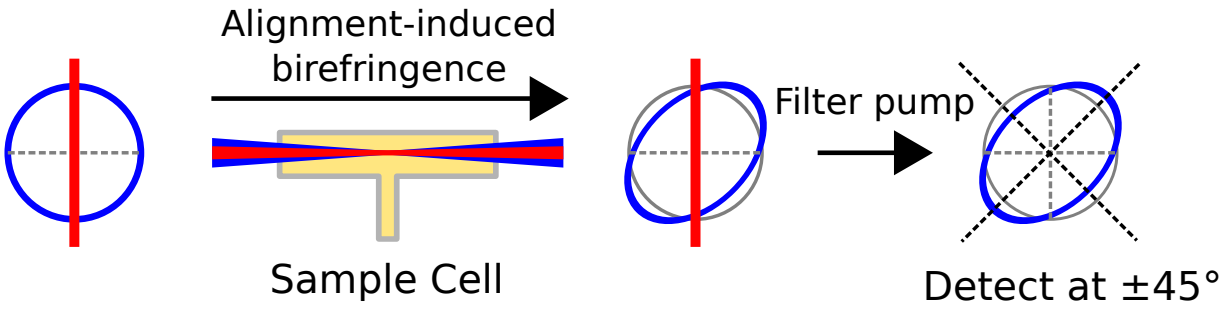

FIG. 3. (Color online) Summary of the polarization-gate scheme for measuring an aligned ensemble. An 800 nm pump pulse (red, vertical line) creates an aligned ensemble, and the alignment is measured at regular time intervals (Δt = 50 fs) by a circularly-polarized 400 nm probe. The anisotropic sample is birefringent, and induces a measurable distortion of the probe polarization.

time-dependent effects, such as anisotropic absorption, that produce signals aligned to the 0° and 90° axes [40].

IV. RESULTS AND ANALYSIS

A. Orientational Decomposition

We model our signal using a version of orientational decomposition approach employed by Spector, et al. [1] adapted to the birefringence polarization-gate measurement. We compute a theoretical time-resolved $\langle \cos^2 \theta \rangle$ signal by propagating the full density matrix given in Equation 5 for a thermal ensemble of SO_2 at 300 K, including a correction for centrifugal distortion, and separate this signal into zero-centered revival traces for $\langle \cos^2 \theta_A \rangle$ and $\langle \cos^2 \theta_B \rangle$. We then model the observed signal by a 9-parameter least-squares fit using the Levenberg-Marquardt algorithm [41]:

$$\begin{aligned} \boldsymbol{\delta}(t)_{SO_2,rev} = \langle \cos^2 \theta_A \rangle_{SO_2,rev}(t - dt) \\ + c_b \cdot \langle \cos^2 \theta_B \rangle_{SO_2,rev}(t - dt) \end{aligned} \tag{8}$$

$$\begin{aligned} \boldsymbol{\delta}(t) = c_{rev} \cdot \boldsymbol{\delta}(t)_{SO_2,rev} \cdot e^{-\frac{(t-dt)}{T_{rev}}} \\ + c_{pop} \cdot e^{-\frac{(t-dt)}{T_{pop}}} \\ + c_{air} \cdot \delta(t - dt_{air})_{air} \cdot e^{-\frac{(t-dt_{air})}{T_{air}}} \end{aligned} \tag{9}$$

Here we combine a SO_2 revival signal ($c_{rev}, c_b, T_{rev}, dt$), a population alignment signal (c_{pop}, T_{pop}), and an air reference signal ($c_{air}, T_{air}, dt_{air}$). The dt and dt_{air} parameters add a temporal offset to allow precise alignment of the signals to the true experimental t_0 (pump-probe temporal overlap). For a more precise fit, we model the air reference using an empirical air signal $\delta(t)_{air}$ measured under identical beam parameters at 295 K and 1.0 bar. This reference signal shows negligible population alignment, and so the parameters c_{pop} and T_{pop} provide good measures of the pure SO_2 population alignment and relaxation rate.

We model the decoherence and population relaxation rates as exponentially-decaying factors ($e^{-(t\,-\,dt)/T_{rev}}$ and $e^{-(t\,-\,dt)/T_{pop}}$) on the revival signal and population alignment. This is equivalent to modeling decoherence and relaxation as first-order processes characterized by

loss of phase coherence ($\rho_{ij}, i \neq j$) and angular momentum (distribution of ρ_{ii}), respectively, to the environment. The true relaxation processes are more complex and include interactions within the excited ensemble, but previous studies have shown that at the high temperature and pressure of this experiment the single-exponential form is a good approximation for the time evolution of the alignment intensity [21, 22, 33].

B. Results

Figure 4 shows the alignment-induced birefringence signal for sulfur dioxide at 0.5 bar and 295 K. We fit the model in the range of 5-27 ps, omitting the strong transient alignment peak. This peak is difficult to fit, as the strong alignment signal "'over-rotates", breaking down the linear approximation of equation 7, and the peak shape experiences additional distortion due to the optical Kerr effect from temporal overlap with the pump pulse. The lower part of Figure 4 shows the pure SO_2 signal, and clearly shows strong J-type revival features corresponding to alignment of the molecular A-axis (prolate axis) with the laboratory frame.

The orientational decomposition model is able to fit the data precisely, and the single-exponential model is able to accurately capture the separate decay rates of the revival signal (phase decoherence) and the population alignment (population relaxation). The population alignment signal is created by an anisotropic distribution of diagonal elements, and decays by transfer of angular momentum through inelastic collisions and internal redistribution of M states. The revival signal is created by coherent phase in the off-diagonal elements, and decays through both inelastic collisions and elastic processes, and will therefore always decay faster than the population. These two rates can be decoupled by the following equation:

$$\frac{1}{T_2^*} = \frac{1}{T_2} - \frac{1}{T_1} = \frac{1}{T_{rev}} - \frac{1}{T_{pop}} \tag{10}$$

where $T_2^* = T_{elastic}$ is the phase lifetime, $T_2 = T_{rev}$ is the revival lifetime, and $T_1 = T_{inelastic} = T_{pop}$ is the population lifetime due to inelastic processes.

We find that the rate of elastic decay ($1/T_2^* = 1/9.62$ ps $= 104$ ns^{-1}) is still much faster than inelastic processes ($1/T_1 = 1/25.64$ ps $= 39$ ns^{-1}), contrary to the trend observed in non-polar diatomics. In particular, experimental studies of diatomic systems including N_2[21] and CO_2[20] have typically found that dissipation in these systems is dominated by inelastic collisions. In such a case, we would expect the rate of phase decoherence to equal

the rate of population relaxation [22, 33], i.e. $1/T_2^* \approx 0$. We find that this is not the case for SO_2, and posit that the large difference in observed lifetimes is related to the presence of a strong permanent molecular dipole ($\mu = 1.63D$ [42]). This dipole is aligned with the SO_2 B-axis, and so in a rotating molecule generates a time-varying field that increases the effective

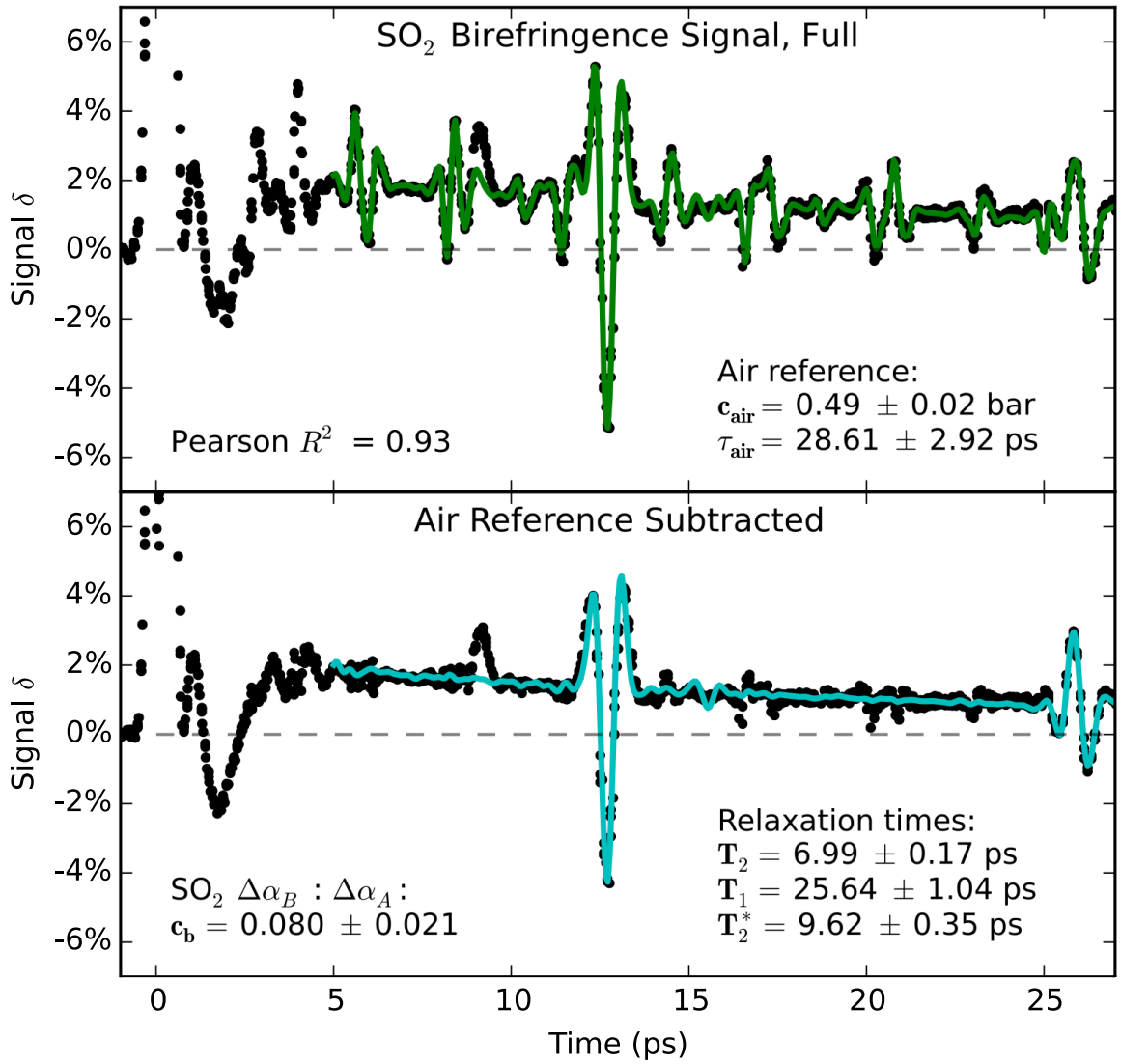

FIG. 4. (Color online) Birefringence trace, 0-27 ps, for sulfur dioxide at 295 K and 0.5 atm. Upper plot is raw trace (black points) fit to full 9-parameter model (green line) as described in Equation 9. Lower plot is the data (black points) and model (blue line) with the air reference ($c_{air} \cdot \delta_{air}(t - dt_{air}) \cdot e^{-\frac{(t-dt_{air})}{T_{air}}}$) term subtracted. The residual feature at 9.2 ps corresponds to the full revival of nitric oxide (NO); see Section IV B for discussion.

interaction cross-section with nearby molecules. This finding, and its generalization to other complex asymmetric top molecules would be important for theories of dissipative processes [22]. Further work remains to study this process in detail, for example by alignment on calibrated mixtures of SO_2 diluted with a noble gas.

We also observe that the rate of population relaxation depends strongly on the degree of excitation. As illustrated in Figure 5, we find a linear relationship ($R^2 = 0.94$) between the magnitude of the population alignment (proportional to the square of the impulse strength) and the population lifetime, and find a strong positive correlation: more highly aligned ensembles also decay more slowly. This agrees well with the trend that has been observed in linear molecules [20–22, 33], which is typically explained by the statistical power-exponential gap law (SPEG) or similar empirical models [43, 44]. These models hold that as energy levels become more widely spaced with increasing J, they become more robust against exchange

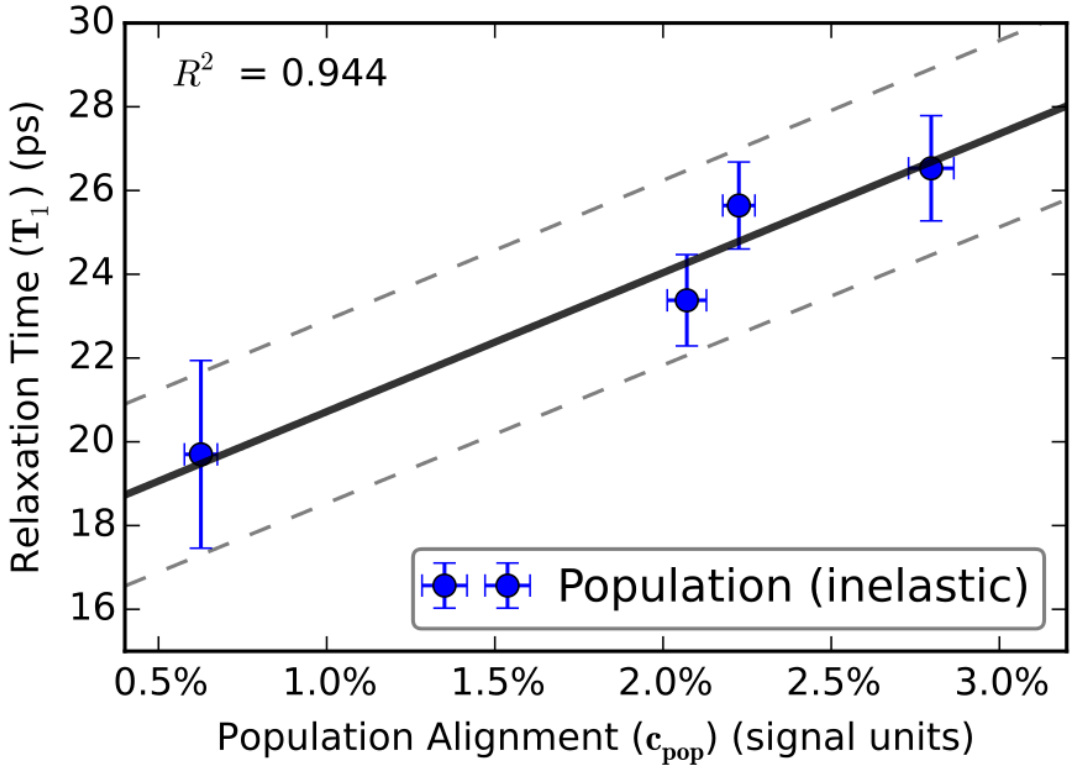

FIG. 5. (Color online) Population lifetime (relaxation time, T_1) as a function of permanent alignment strength (c_{pop}), as measured across four datasets taken with pump energies between 24 μJ and 48 μJ ($22 - 55$ TW/cm^2) on the same 0.5 bar, 295 K sample of SO_2.

of angular momentum through collisional processes. Out results suggest that a similar relationship holds in an asymmetric top as well, which suggests that the pursuit of high levels of alignment through multiple pulses and other techniques is not only a route toward strong transient alignment, but also a viable means to achieve long-lived rotationally coherent ensembles.

Additionally, by fitting an exponential decay factor to the background air signal in our measurement, we observe that the amplitude of the O_2 and N_2 revivals in the presence of SO_2 decay at a rate ($T_{air} \approx 22$ps) nearly three times that of pure N_2 ($T_{N_2} > 60$ ps [21]) under similar conditions. We attribute this to intermolecular coupling between sulfur dioxide and O_2 and N_2, mediated by the SO_2 permanent dipole, which rotates with the ensemble to create an oscillating quadrupole field.

Finally, we note the presence of a strong residual at 9.2 ps, which corresponds to the first full revival of nitric oxide (NO). We identify this as an impurity, accumulating as the result of inadvertent photoionization of the air reference (N_2 + O_2) in our sample cell during the course of our experiment. NO is a diatomic molecule with a permanent dipole ($\mu = 0.16$ D [42]), which we expect to couple strongly to the field of the SO_2 dipole. This results in rapid decoherence, and explains the absence of the 3/2- and subsequent revivals that would otherwise be seen in an impulsively-aligned linear molecule.

V. CONCLUSION

We provide a complete model for all features of the alignment signal, and show through the combination of experiments with theory, that the orientational decomposition method allows us to subtract background signals and can account for rapid decoherence and relaxation of the rotational wavepacket. The birefringence polarization-gate measurement provides a low-noise linear signal that, unlike vacuum-based techniques such as HHG and Coulomb explosion imaging, is well-suited to studying dense ensembles. Moreover, it is a non-destructive technique that can be applied to a wide range of molecules. We are able to measure all the non-idealities of asymmetric-top rotational dynamics, including asymmetric top couplings, phase decoherence, population relaxation, and multiple-axis contributions, and to quantify these effects over the timescale of a full rotational "period".

This work demonstrates that experimental control of asymmetric-top rotational wavepack-

ets is possible over tens-of-ps timescales, and that rates of alignment decoherence can be used to independently measure the contributions of elastic and inelastic collisions. This agrees with the theoretical work of [22, 33], and with past experimental demonstrations of this work in linear molecules. We demonstrate that population relaxation slows with increasing alignment, which suggests that efforts toward achieving high levels of peak alignment in asymmetric tops may also permit the study of wavepackets with longer lifetimes. In the rapid decoherence of the background air signal, we find evidence for intermolecular dipole interactions that can be studied through their effects on the rotational wavepacket, and we suggest that these effects, particularly when measured over multiple rotational periods, provide a powerful means to study quantum control of chemical reactions.

Further work remains to understand the connection between elastic collision processes and our observed decoherence rates, as this is typically modeled as an empirical parameter $\gamma^{(pd)}$ (Section IV B) and has not been well-studied in the context of asymmetric top revivals. Furthermore, more theoretical work could illuminate the mechanism of cross-species coupling, and improve our understanding of how angular momentum is transferred through collisions and long-range dipole interactions. Nonetheless, we emphasize that it is indeed feasible to observe strong quasi-revivals in an asymmetric top at high temperature and density, and that these features provide a rich source of molecular-frame data for studying HHG and other anisotropic molecular properties.

ACKNOWLEDGMENTS

The authors would like to thank Limor Spector, James Cryan, Brian K. McFarland, Song Wang, and Markus Guehr for their helpful discussions. Tamar Seideman thanks the Department of Energy (grant DE-FG02-04ER15612) for support. Ian Tenney was supported by the National Science Foundation (grant PHY-0969322).

[1] L. S. Spector, M. Artamonov, S. Miyabe, T. Martinez, T. Seideman, M. Guehr, and P. H. Bucksbaum, Nature communications **5**, 3190 (2014).

[2] P. H. Bucksbaum, Science **317**, 766 (2007).

[3] P. B. Corkum and F. Krausz, Nature Physics **3**, 381 (2007).

[4] J. Itatani, J. Levesque, D. Zeidler, H. Niikura, H. Ppin, J.-C. Kieffer, P. B. Corkum, and D. M. Villeneuve, Nature **432**, 867 (2004).

[5] B. K. McFarland, J. P. Farrell, P. H. Bucksbaum, and M. Ghr, Science **322**, 1232 (2008).

[6] N. Kajumba, R. Torres, J. G. Underwood, J. S. Robinson, S. Baker, J. W. G. Tisch, R. de Nalda, W. A. Bryan, R. Velotta, C. Altucci, and others, New Journal of Physics **10**, 025008 (2008).

[7] H. J. Worner, J. B. Bertrand, D. V. Kartashov, P. B. Corkum, and D. M. Villeneuve, Nature **466**, 604 (2010).

[8] V. Renard, M. Renard, S. Guerin, Y. T. Pashayan, B. Lavorel, O. Faucher, and H.-R. Jauslin, Physical review letters **90**, 153601 (2003).

[9] V. Renard, M. Renard, A. Rouzee, S. Guerin, H.-R. Jauslin, B. Lavorel, and O. Faucher, Physical Review A **70**, 033420 (2004).

[10] J. P. Cryan, P. H. Bucksbaum, and R. N. Coffee, Physical Review A **80**, 063412 (2009).

[11] D. W. Broege, R. N. Coffee, and P. H. Bucksbaum, Physical Review A **78**, 035401 (2008).

[12] P. M. Felker, The Journal of Physical Chemistry **96**, 7844 (1992).

[13] E. Peronne, M. D. Poulsen, C. Z. Bisgaard, H. Stapelfeldt, and T. Seideman, Physical review letters **91**, 043003 (2003).

[14] M. Artamonov and T. Seideman, Physical Review A **82**, 023413 (2010).

[15] S. Pabst and R. Santra, Physical Review A **81**, 065401 (2010).

[16] M. Artamonov and T. Seideman, Molecular Physics **110**, 885 (2012).

[17] A. Pelzer, S. Ramakrishna, and T. Seideman, The Journal of chemical physics **129**, 134301 (2008).

[18] M. Lapert, E. Hertz, S. Guerin, and D. Sugny, Physical Review A **80**, 051403 (2009).

[19] X. Ren, V. Makhija, and V. Kumarappan, Physical Review Letters **112**, 173602 (2014).

[20] T. Vieillard, F. Chaussard, D. Sugny, B. Lavorel, and O. Faucher, Journal of Raman Spectroscopy **39**, 694 (2008).

[21] N. Owschimikow, F. Knigsmann, J. Maurer, P. Giese, A. Ott, B. Schmidt, and N. Schwentner, The Journal of chemical physics **133**, 044311 (2010).

[22] S. Ramakrishna and T. Seideman, Physical review letters **95**, 113001 (2005).

[23] K. F. Lee, D. M. Villeneuve, P. B. Corkum, A. Stolow, and J. G. Underwood, Physical review letters **97**, 173001 (2006).

[24] J. H. Mun, D. Takei, S. Minemoto, and H. Sakai, Physical Review A **89**, 051402 (2014).

[25] M. D. Poulsen, E. Peronne, H. Stapelfeldt, C. Z. Bisgaard, S. S. Viftrup, E. Hamilton, and T. Seideman, The Journal of chemical physics **121**, 783 (2004).

[26] L. Holmegaard, S. S. Viftrup, V. Kumarappan, C. Z. Bisgaard, H. Stapelfeldt, E. Hamilton, and T. Seideman, Physical Review A **75**, 051403 (2007).

[27] S. S. Viftrup, V. Kumarappan, S. Trippel, H. Stapelfeldt, E. Hamilton, and T. Seideman, Physical review letters **99**, 143602 (2007).

[28] S. S. Viftrup, V. Kumarappan, L. Holmegaard, C. Z. Bisgaard, H. Stapelfeldt, M. Artamonov, E. Hamilton, and T. Seideman, Physical Review A **79**, 023404 (2009).

[29] G. Paterson, S. Marinakis, M. L. Costen, K. G. McKendrick, J. Kos, and R. Toboa, The Journal of Chemical Physics **129**, 074304 (2008).

[30] M. Brouard, H. Chadwick, Y.-P. Chang, R. Cireasa, C. J. Eyles, A. O. L. Via, N. Screen, F. J. Aoiz, and J. Kos, The Journal of Chemical Physics **131**, 104307 (2009).

[31] H. Stapelfeldt and T. Seideman, Reviews of Modern Physics **75**, 543 (2003).

[32] T. Seideman and E. Hamilton, Advances in atomic, molecular, and optical physics **52**, 289 (2006).

[33] S. Ramakrishna and T. Seideman, The Journal of chemical physics **124**, 034101 (2006).

[34] J. G. Underwood, B. J. Sussman, and A. Stolow, Physical review letters **94**, 143002 (2005).

[35] A. R. Edmonds, *Angular momentum in quantum mechanics /*, 3rd ed. (Princeton, N.J. : Princeton University Press,, 1974).

[36] R. N. Zare, *Angular momentum : understanding spatial aspects in chemistry and physics /* (Wiley,, New York :, 1988).

[37] See Appendix A of [32] for a thorough derivation.

[38] National Institute of Standards and Technology, "NIST chemistry WebBook," (2014), accessed: July 2014.

[39] National Institute of Standards and Technology, "NIST computational chemistry comparison and benchmark (2013), accessed: July 2014.

[40] For this reason, it is not necessary to use a *probe* frequency far from any electronic transitions; direct absorption will be a common-mode signal in the $\pm 45^\circ$ channels.

[41] D. W. Marquardt, Journal of the Society for Industrial & Applied Mathematics **11**, 431 (1963).

[42] Taylor and Francis Group, LLC, *CRC Handbook of Chemistry and Physics, 95th Edition*

(2014) accessed: July 2014.

[43] A. E. Belikov and M. A. Smith, The Journal of chemical physics **110**, 8513 (1999).

[44] L. Bonamy, J. Bonamy, D. Robert, B. Lavorel, R. Saint-Loup, R. Chaux, J. Santos, and H. Berger, The Journal of chemical physics **89**, 5568 (1988).